Published in final edited form as:
Curr Biol. 2009 July 14; 19(13): 1065–1074. doi:10.1016/j.cub.2009.05.065.

Par3 and dynein associate to regulate local microtubule dynamics and centrosome orientation in migrating cells

J. Schmoranzer[1], **J. P. Fawcett**[2], **M. Segura**[1], **S. Tan**[1], **R. B. Vallee**[1], **T. Pawson**[3], and **G. G. Gundersen**[1,4]

[1]Department of Pathology and Cell Biology, Columbia University, New York, NY, US

[2]Department of Pharmacology and Surgery, Dalhousie University, Halifax, NS, Canada

[3]Samuel Lunenfeld Research Institute, Mount Sinai Hospital, Toronto, ON, Canada

Summary

Background—Centrosome orientation toward the leading edge of migrating cells depends on dynein and microtubules (MTs) and as well on a number of signaling factors at the leading edge. However, centrosomes are maintained at the cell center during orientation in fibroblasts suggesting that factors working at sites other than the leading edge may also be involved.

Results—In a search for factors that function with dynein in centrosome orientation, we found that the polarity protein Par3 associated with dynein and that knockdown of Par3 inhibited centrosome orientation by disrupting the position of the centrosome at the cell center, the same phenotype as that observed with dynein inhibition. Par3 associated with dynein through its N-terminal dimerization and PDZ1 domains, and interacted specifically with dynein light intermediate chain 2 (LIC2). siRNA knockdown of LIC2, but not LIC1, or overexpression of LIC2 or the N-terminal domain of Par3, also inhibited centrosome orientation by disrupting centrosome position. Par3 specifically localized to cell-cell contacts in wound-edge fibroblasts where it overlapped with MT ends and dynein puncta in a LIC2 dependent fashion. Live imaging showed that MTs exhibited increased pausing at cell-cell contacts compared to the leading edge and that this elevated pausing was dependent on Par3 and LIC2.

Conclusion—Par3 associates with dynein and contributes to the local regulation of MT dynamics at cell-cell contacts and proper positioning of the centrosome at the cell center. We propose that Par3 acts as a cortical factor that tethers MTs through its association with LIC2-dynein.

Introduction

In many directionally migrating cell types including fibroblasts, endothelial cells, astrocytes, and neurons, the centrosome that gives rise to the MT organizing center becomes oriented between the nucleus and the leading edge [1-5]. The orientation of the centrosome contributes to overall cell polarity by positioning both the Golgi and the endocytic recycling compartment between the nucleus and leading edge to direct membrane traffic from both compartments toward the leading edge [6-8].

[4]Corresponding Author: Gregg G. Gundersen, Department of Anatomy and Cell Biology, 630 West 168th Street, BB 1217, New York, NY, 10032, T- 212-305-1899, F- 212-305-3970, ggg1@columbia.edu

The microtubule minus-end motor dynein plays an important role in centrosome orientation in several migrating cell types [1-3,9]. Dynein is localized to the leading edge in migrating cells, suggesting that it may exert force from this site to move the centrosome toward the leading edge during orientation [10]. However, we recently found that the centrosome remains at the cell center while the nucleus moves rearward during centrosome orientation in wound-edge fibroblasts [9]. Dynein and MTs are still important for centrosome orientation as inhibition of dynein or MTs results in rearward displacement of the centrosome from the cell center [9]. Coupled with similar findings from sparse cells [11], these results indicate that an active MT- and dynein-dependent process maintains the centrosome in the center during orientation.

There are models for dynein function during centrosome orientation [11-13], yet it is unclear where dynein functions in the cortex and how it is targeted to cortical sites. In astrocytes and fibroblasts, dynein functions downstream of the polarity protein Par6 and its binding partner aPKC, yet at least in astrocytes, these factors are thought to function at the leading edge to regulate MTs through GSK3β and APC and are not known to regulate dynein function [1,2, 9]. Par6/aPKC and other Par proteins function to asymmetrically position the mitotic spindle (and hence centrosomes) in the *C. elegans* zygote [14,15]. Dynein also participates in spindle/centrosome positioning in the *C. elegans* zygote and may generate pulling forces at cortical sites that are exerted on MTs in this system [13,16,17]. Although a molecular link between the Par proteins and dynein has not been identified, Par3 and Par2 are known to locally regulate cortical MT resident times in *C. elegans* [18]. Here, we explore Par3's role in centrosome orientation in wound-edge migrating cells, its relationship to dynein and how it affects the MT dynamics.

Results

Par3 associates with dynein

In searching for factors that might couple dynein to cortical sites for centrosome orientation, we found that dynein associated with Par3. Par3 co-immunoprecipitated with anti-dynein intermediate chain antibody (αDIC) from NIH3T3 cell lysates. Both the 180 kDa and 100 kDa isoforms of Par3 expressed in NIH3T3 cells immunoprecipitated with αDIC. Other proteins implicated either in cell polarity or centrosome orientation (Par6, aPKC, Lgl-1 [1,9,19-21]) or as cortical dynein interacting proteins (β-catenin [22]), did not, or only weakly (PKCζ), co-immunoprecipitated with dynein (Figure 1A). Dynactin has been implicated in centrosome orientation [2], but the $p150^{Glued}$ subunit of dynactin was not detected in αDIC immunoprecipitates (Figure 1A). Par3 is likely associated with dynein holoenzyme as αDIC immunoprecipitates dynein holoenzyme [23] and we observed dynein heavy chains (DHC) and light intermediate chains (LICs) in the immunoprecipitates (Figure 1A and data not shown). Two different Par3 antibodies failed to coimmunoprecipitate dynein perhaps because the antibody epitopes lie within regions that interact with dynein or other proteins (data not shown). Instead, we expressed YFP-Par3 in COS-7 cells and immunoprecipitated with anti-GFP antibody, which recognizes YFP. Dynein was detected in YFP-Par3 immunoprecipitates supporting the notion that the two proteins associate in cells (Figure 1B).

To investigate the region(s) of Par3 that associated with dynein, we immunoprecipitated dynein from COS-7 cells transfected with YFP-Par3 fragments (Figure 1C). Par3 full length and Par3 N-terminal (Nt-90, Nt-205, Nt-283) or PDZ1 (PDZ1 205-477) fragments coimmunoprecipitated with dynein whereas Par3 PDZ2+3 or C-terminal fragments did not. Thus, the association of dynein with Par3 involves specific regions of Par3.

Cytoplasmic dynein is a large (> 1 MDa) complex composed of dimers of DHCs, DICs, LICs, and light chains [24]. To identify dynein subunit(s) that associated with Par3, we co-expressed individual tagged dynein subunits with YFP-Par3 in COS-7 cells and immunoprecipitated

YFP-Par3 [25]. Since exogenous dynein subunits are expressed in excess of endogenous dynein, they are free to interact with targeting proteins [25]. Only LIC2, but not DHC, DIC, or LIC1, and to a lesser extent the related light chains, Tctex-1 and Rp3, co-immunoprecipitated with YFP-Par3 (Figure 1D). We tested whether the interaction between dynein and Par3 was direct using GST-tagged N-terminal and PDZ1 Par3 fragments and purified brain dynein, but did not detect any binding, suggesting that posttranslational modifications or other proteins may be involved in the association (data not shown). We conclude that LIC2, but not LIC1, and perhaps Tctex-1 and Rp3, contribute to the association of Par3 and dynein.

Par3 is necessary for centrosome orientation and centration

To assess whether Par3 participates in centrosome orientation we depleted Par3 in NIH3T3 cells using siRNA. Separate siRNA sequences reduced Par3 in NIH3T3 cells 4-fold (#1) and 2-fold (#2) compared to control cells (Figure 2A and Figure S1A,B in the Supplementary Data available online). Par3 isoforms were reduced to similar levels in NIH3T3 cells and a NIH3T3 cell line stably expressing GFP-α-tubulin (Figure 2A). In NIH3T3 cells, Par3 localized to cell-cell contacts, but in Par3 depleted cells, only very low levels of Par3 were detected (Figure 2B). Par3 depletion did not affect the localization of junctional markers (β-catenin or N-cadherin) suggesting that cell-cell contacts were not affected (Figure 2B and data not shown).

We next evaluated whether Par3-depleted, serum-starved NIH3T3 cells were capable of orienting their centrosome in response to LPA [2]. Par3 depletion, but not GAPDH depletion (control) inhibited LPA-stimulated centrosome orientation to a similar extent as cells injected with αDIC (Figure 2C)[2,9]. Two siRNAs targeting Par3 inhibited centrosome orientation showing that the inhibition was not due to off-target effects (Figure S1C).

We next examined whether Par3 depletion affected actin-dependent rearward movement of the nucleus and/or dynein/MT-dependent maintenance of the centrosome at the cell centroid, both of which are required for centrosome orientation in NIH3T3 cells [9]. As reported previously, LPA stimulated control cells positioned the nucleus rearward from the cell centroid while the centrosome stayed at the cell centroid (Figure 2D). In Par3 depleted cells, the nucleus was positioned rearward, however, the centrosome did not remain at the cell centroid but instead was positioned rearward with the nucleus (Figure 2D and S1D). This centrosome phenotype is similar to that observed for dynein inhibition (Figure 2D) [9], suggesting that Par3 and dynein are in the same pathway for centrosome orientation.

To test whether Par3-dynein association is important for centrosome orientation, we expressed YFP-Par3 fragments in serum-starved wound-edge NIH3T3 cells and then stimulated centrosome orientation with LPA (Figure 2E). Expression of three Par3 fragments (Nt-90, Nt-283, PDZ1) that interacted with dynein inhibited centrosome orientation compared to a Par3 fragment (205-283) that did not bind to dynein (Figure 2F). Par3-Nt-90 and Nt-283 disrupted centrosome positioning at the cell center, but not rearward nuclear positioning, whereas Par3-PDZ1 partially inhibited nuclear movement (Figure 2G). No effect on nuclear positioning was observed with the non-interacting fragment (Figure 2G). We conclude that Par3 fragments that associate with dynein block overall centrosome orientation and that at least the N-terminal fragments primarily affect dynein-dependent centrosome positioning. Defects in centrosome positioning can only be detected if the nucleus moves rearward, so the inhibition of nuclear movement with the PDZ1 fragment could mask a defect in centrosome positioning. We note that the PDZ1 domain of Par3 has multiple interaction partners and interfering with these interactions may have secondary effects.

Dynein LIC2 is necessary for centrosome orientation and centration

Dynein LICs exhibit mutually exclusive binding to the dynein complex [26]. Our findings raised the possibility that the LIC2 pool of dynein is specifically involved in centrosome orientation. To test this possibility, we depleted LIC1 and LIC2 with specific siRNAs. Two siRNAs for each LIC specifically reduced the targeted LIC about 3-fold in NIH3T3 cells without reducing the related isoform (Figure 3A and S2A,B). The level of DIC was unaffected by LIC knockdowns, suggesting that LICs are not essential for dynein holoenzyme stability (Figure S2C).

Depletion of LIC2, but not of LIC1, specifically inhibited centrosome orientation stimulated by LPA (Figure 3B,C). Knocking down both LICs did not further inhibit centrosome orientation. LIC2 depletion caused centrosome displacement from the cell center due to rearward positioning with the nucleus, whereas LIC1 depletion had no affect on centrosome positioning (Figure 3D). Neither LIC1 nor LIC2 depletion affected rearward positioning of the nucleus (Figures 3D and S2D,E). These data show that LIC2 specifically functions in centrosome orientation and contributes to positioning of the centrosome, but not the nucleus.

If LIC2 association with Par3 is important for centrosome orientation, then overexpression of LIC2 may act as a dominant negative by preventing Par3 association with holoenzyme dynein. Indeed, overexpression of LIC2 blocked centrosome orientation with a similar centrosome positioning defect as that observed for Par3 depletion, Par3-Nt overexpression or αDIC injection (Figure 3E-G). Together, these data show that the Par3-binding dynein subunit LIC2 is specifically involved in centrosome orientation through maintenance of the centrosome at the cell center.

Depletion of Par3 causes a migratory defect

Par3 depletion caused a defect in centrosome orientation, so we tested whether Par3 was also required for directed migration into *in vitro* wounds. Since LPA stimulates orientation, but not migration into wounds, we examined whether knockdown of Par3 interfered with serum-stimulated migration of cells. Par3 knockdown inhibited centrosome orientation stimulated by serum, although the inhibition was not as complete as when stimulated by LPA: in serum, centrosome orientation was 44.5% +/- 9.5% in Par3 depleted cells vs. 63.5% +/- 7.4% in control GAPDH depleted cells. The Par3 depleted cells showed decreased wound closure and rate of migration compared to control cells (Figure 4A,B). Because the Par3 knockdown was incomplete, we also tested whether expression of dominant negative Par3-Nt-90 in wound edge cells affected migration. Most cells expressing Par3-Nt-90 fell behind non-expressing cells migrating into the wound (Figure 4C,D). In contrast, most of the cells expressing the control Par3 205-283 remained at the wound edge (Figure 4C,D). These data are consistent with studies of other cell types that have shown a moderate effect of Par3 on cell migration [27, 28].

Par3 localizes to cell-cell contacts in wound-edge fibroblasts where it overlaps MT ends and dynein

The localization of Par3 is critical for its function in polarization [14]. Previously, Par3 has been localized to cell-cell contacts of confluent NIH3T3 cells [29]. We found that endogenous Par3 is prominently localized to cell-cell contacts, and in small puncta scattered throughout the cell, but not the leading edge of LPA- or serum-stimulated wound-edge NIH3T3 cells (Figure 5A,C). Par3 at cell-cell contacts colocalized with junctional markers (Figure S3). Par3 localization to cell-cell contacts depended on intact contacts between cells: upon wounding, Par3 disappeared within minutes from the contact-free leading edge (data not shown). Both Par6 and aPKC were diffusely distributed in NIH3T3 cells and did not accumulate at the leading edge (Figure S4). As previously reported, some of the Par3 at cell-cell contacts in NIH3T3

cells colocalized with aPKC [29] (Figure S4B), whereas in polarized MDCK epithelial cells they were strongly colocalized [14] (data not shown).

In starved NIH3T3 cells, LPA stimulated a rearrangement of Par3 from linear structures parallel to cell-cell contacts to zipper-like structures perpendicular to cell-cell contacts (Figures 5A,C and S3). In starved cells at the wound edge, the ends of MTs rarely overlapped with Par3 at cell-cell contacts (Figure 5B and S5). In contrast, in LPA-stimulated cells, many MT ends overlapped with Par3 puncta at cell-cell contacts (Figure 5D and S5). Quantification of this Par3/MT overlap showed a significant increase upon LPA stimulation (Figure 5E). Importantly, this increased overlap was significantly diminished in LIC2, but not LIC1, depleted cells (Figure 5E and S5).

We also colocalized Par3 and dynein in LPA-stimulated wound-edge NIH3T3 cells. Consistent with an earlier study, dynein puncta were localized throughout the cell with prominent localizations in the perinuclear area and some accumulation at the leading edge (Figure 5F) [10]. In addition, we detected dynein puncta in cell-cell contact areas where they frequently formed short linear or curvilinear streaks (Figure 5G and S6). Some dynein puncta colocalized with Par3 puncta near cell-cell contacts (Figure 5G). Quantification showed a significant increase in Par3/dynein overlap upon LPA stimulation (Figure 5H). Importantly, in LIC2, but not LIC1, depleted cells, the Par3/dynein overlap was reduced to unstimulated levels (Figure 5H and S6). The colocalization of Par3 with MTs and dynein suggests that Par3 may interact with dynein to tether MTs at these sites.

Par3 and LIC2 locally regulate MT dynamics at cell-cell contacts

The interaction between Par3 and dynein, and the overlap of Par3 with MTs and dynein near cell-cell contacts, suggested that Par3 may affect MTs at these sites. Previous studies have observed reduced MT dynamics near cell-cell contacts or at cell-sides in migrating cells, although the molecular mechanism involved was not identified [30,31]. We explored this issue by measuring MT dynamics at both cell-cell contacts and the leading edge in wound-edge NIH3T3 cells stably expressing GFP-α-tubulin (Figure 6A and Supplementary Movies 1-10).

In starved cells MTs at cell-cell contacts and the leading edge exhibited typical dynamic instability with periods of growth and shortening interspersed with short pausing intervals (Figure 6B). As a population, MTs spent ~40% of their total time pausing (neither growing nor shortening) at both cell-cell contacts and the leading edge (Figure 6C). After LPA stimulation, MT pausing increased, particularly at cell-cell contact areas (Figure 6B). Quantification revealed that LPA stimulated a highly significant increase in MT pausing at cell-cell contacts (to 71% of total time) and at the leading edge (to 51 % of total time) (Figure 6C). Thus, the time that MTs spent pausing after LPA stimulation increased 80% at cell-cell contacts but only 20% at the leading edge (Figure 6C).

Consistent with LPA-stimulated changes in MT pausing, we observed a reciprocal change in MT dynamicity, which measures overall MT dynamic behavior. (Supplementary Data, Table 1). Beside increased MT pausing, the only other highly significant difference was in MT shortening rates. However, LPA treatment decreased shortening rates at both cell-cell contacts and the leading edge (Supplementary Data, Table 1). We conclude that LPA selectively affects MT pausing at cell-cell contacts and shortening rates more globally. The small LPA-stimulated increase in MT pausing at the leading edge was previously reported and is likely to reflect the formation of a small subset of long-lived stable MTs [32].

To determine whether the increased MT pausing was due to longer individual pauses and/or a greater number of MTs pausing, we measured the length of individual MT pauses. In starved cells, ≥ 90% of the pause events at either the leading edge or cell-cell contact regions were less

than 30 sec, whereas in LPA-stimulated cells there was a ~25% increase in MTs that exhibited pauses longer than 30 sec (Figure 6D). MTs that paused longer than 30 sec increased slightly (1.3-fold) at the leading edge, but dramatically (5-fold) at the cell-cell contacts (Figure 6D). Thus, LPA activates pausing at cell-cell contacts resulting in a regional reduction of MT dynamics.

We next measured MT dynamics in LPA-treated cells depleted of Par3 or one of the LICs. Par3 knockdown selectively affected MT pausing at the cell-cell contacts compared to the GAPDH depleted controls. Life history plots of individual MTs at cell-cell contacts in Par3 depleted cells revealed that MTs no longer exhibited long intervals of pause but instead exhibited dynamics that resembled those in serum-starved cells (Figure S7). Par3 depletion reduced MT pausing at cell-cell contacts to the levels observed at the leading edge without affecting pausing at the leading edge (Figure 6C,D). LIC2 knockdown also selectively affected MT pausing at the cell-cell contacts, without affecting pausing at the leading edge (Figure 6C,D). Consistent with increased MT pausing, Par3 and LIC2 knockdown decreased MT dynamicity at cell-cell contacts (Supplementary Data, Table 1). In contrast, depletion of LIC1 only partially reduced pausing at the cell-cell contacts and actually increased pausing at the leading edge (Figure 6C,D). We also observed small, but significant, changes in growth and shortening rates with depletion of individual proteins, particularly LIC2, but none of these seemed to reflect regional differences in MT dynamics (Supplementary Data, Table 1).

To test whether increased MT pausing reflected Par3 association with dynein, we expressed dynein-interacting YFP-Par3-Nt-90 in cells and measured MT dynamics by co-injecting Cy3-labeled tubulin. The total time MTs paused and the percentage of long-paused MTs at cell-cell contacts were significantly reduced in YFP-Par3-Nt-90 expressing cells compared to cells expressing a Par3 fragment that did not interact with dynein (Figure 6E,F). Expression of either fragment of Par3 did not significantly affect MT pausing at the leading edge (data not shown). These data demonstrate a novel function for Par3 and LIC2-dynein in regionally controlling MT pausing at cell-cell contacts.

Discussion

We identified the polarity protein Par3 as a novel factor involved in centrosome orientation in migrating mammalian fibroblasts. Supporting this conclusion, we showed that Par3 associated specifically with dynein, and that Par3 knockdown and dominant negative expression interfered with centrosome orientation by disrupting centrosome centration, which is characteristic of proteins that function with dynein in centrosome orientation [9]. The similarities of the Par3 and LIC2 depletion phenotypes on centrosome orientation and MT dynamics strongly suggest that Par3 mediates its effect on the MT cytoskeleton via a specific association with LIC2 containing dynein.

It has been postulated that centrosome orientation requires movement of the centrosome toward the leading edge and this has focused attention on events at the leading edge [10,33]. However, in LPA-stimulated fibroblasts, the nucleus moves rearward while the centrosome is maintained in the cell center [9]. This finding raises the possibility that factors at sites other than the leading edge act on MTs to maintain the centrosome in the cell center. Our current results suggest that interactions of MTs with cell-cell contact sites contribute to centrosome orientation. The enhanced pausing of MTs at cell-cell contacts during LPA stimulation most likely reflects increased interaction of MTs with cell-cell contact sites. Based upon the Par3 and LIC2-dependence of this pausing and the LIC2-dependence of LPA-stimulated MT and dynein overlap with Par3 at cell-cell contacts, we propose that Par3 and dynein tether MTs at cell-cell contacts. Such tethering may contribute to centrosome position by allowing dynein to generate tension (or pulling) on MT ends. Alternatively, tethering of MTs may simply anchor MTs so

that they can resist forces that may displace the centrosome from the cell center. Since cell-cell contacts occur both in front of and behind the centrosome, such tethering would prevent the displacement of the centrosome rearward by actin retrograde flow. The pool of dynein at the leading edge may also contribute to centering the centrosome [10], yet our data stress the need to consider cell-cell contacts as sites where MT/cortical interactions help to position the centrosome.

Regional differences in MT dynamics in migrating cells are known [30,31], but the molecular basis for these differences and their functional consequences are incompletely understood. Our data show that both Par3 and LIC2 specifically contribute to regulation of MT dynamics at cell-cell contacts. In particular, both proteins are necessary for the LPA-stimulated increase in pausing at cell-cell contacts. Further, expression of the Par3-Nt90 fragment that associated with dynein and blocked centrosome orientation also reduced MT pausing at cell-cell contacts. That all three treatments had the same effect on centrosome orientation and MT pausing strongly suggests that the Par3/dynein association is important for both centrosome orientation and the local regulation of MT dynamics. Par3 and Par2 regulate MT cortical residence times in *C. elegans* embryos [18], suggesting that local regulation of MT dynamics is a conserved function for Par proteins.

Dynein has been implicated in controlling MT dynamics at cortical sites, although previous studies have not unambiguously identified a “cortical receptor” for dynein. Num1 appears to be a cortical anchor for dynein in yeast although its role in regulating MT dynamics in yeast has not been explored [34]. In mammalian epithelial cells, dynein inhibition prevents the end-on interaction of MTs with cell-cell junctions, although the possibility that dynein may regulate MT pausing at these sites has not been tested [35]. Our data are the first to demonstrate that a cortical protein, Par3, is necessary for regional control of MT dynamics along with LIC2, suggesting that Par3 may be a ‘cortical receptor’ for dynein in mammalian cells. It will be important for future experiments to determine mechanistically how dynein and its putative cortical receptors lead to changes in MT dynamics.

While LIC1 is known to specifically bind pericentrin [25,26], our report is the first to demonstrate a LIC2-specific association (with Par3) and function (in centrosome orientation). Combined with earlier data showing that both LIC1 and LIC2 form homodimers that exhibit mutually exclusive binding to the dynein heavy chain, our data support the idea that mammalian LICs target pools of dynein for specific functions or localizations [25,26].

In many systems, Par3 is both functionally and physically linked to the polarity protein complex Par6/aPKC [14]. However, there are numerous systems where Par3 is not associated with the Par6/aPKC complex [36-38] or where Par3 and Par6 contribute to the same process through separate pathways [39,40]. We find that Par3 associates with dynein in the absence of Par6 and with only a small amount of PKCζ (Figure 1A). Further, PKCζ only weakly co-localized with Par3 at cell-cell contacts in NIH3T3 cells (Figure S4B, see also [29]) while Par6 was not detectable at cell-cell contacts (Figure S4). Given these data, it is possible that Par3 and dynein associate and mediate their effects on MTs at cell-cell contacts independently of Par6/PKCζ. Perhaps because Par6 and dynein both interact with the PDZ1 domain of Par3, the interaction of Par3 with dynein and Par6 is mutually exclusive.

We are only starting to understand the complex molecular connections between the Par proteins and the cytoskeleton [14,40]. Our study suggests that at least one of these connections involves a unique association between Par3 and LIC2-dynein. In the future it will be interesting to explore how other Par proteins, such as Par1 and Par2, both of which have been implicated in regulation of MTs [18,41], may form connections with the MT cytoskeleton.

Experimental Procedures

Reagents

Mouse mAb αDIC (mAb 74.1) was from Chemicon (Temecula, CA). Rabbit antibodies to DHC and LIC2 were described previously [26,42]. Chicken antibody against a LIC1 peptide will be described elsewhere (Tan and Vallee, manuscript in preparation). Mouse antibodies to p150^{Glued} and mDia1 were from BD Biosciences. Rabbit antibodies to Par3 (affinity purified), Par6C, Lgl-1 were previously described [20,21]. Rabbit anti-Par3 (commercial source) was from Upstate (Lake Placid, NY). Rabbit anti-PKCζ and Myc (9E10) mAb were from Santa Cruz Biotechnology (Santa Cruz, CA). Rat anti-tyrosinated α-tubulin (mAb YL1/2) was from the European Collection of Animal Cell Cultures (Salisbury, UK). Mouse mAbs β-catenin andto N-cadherin were from Zymed Laboratories (San Francisco, CA). Rabbit anti-Flag was from Affinity Bioreagents (Golden, CO). Rat anti-HA (12CA5) mAb was from Roche (Indianapolis, IN). Rabbit anti-GFP was from BD Biosciences (Palo Alto, CA). Mouse anti-GFP and anti-vinculin mAb were from Sigma. All other chemicals were from Sigma.

Most YFP-tagged mPar3 (full-length and fragments in pEYFP-C1 vector (Clontech, Mountain View, CA) were previously described [20,21]. The YFP-Par3 fragments (Nt-90, Nt-205, 205-283) were cloned from the YFP-mPar3 100kDa. For YFP-Par3 Nt-90, YFP-mPar3 100kDa plasmid was cut with EcoR1 and Kpn1, the Kpn1 site was removed and religated. Primers for Nt-205 were: (Forward (EcoR1) TTT GCT TCG AAT TCT ATG AAA GTG ACC; Reverse (Sal1) TTT GTC GAC TGG TTA ATC CCG TGG AAG GCT). Primers for 205-283 were: (Forward (EcoR1) GCT TCG AAT TCT GAT CCC AGT AGC TGG; Reverse (Sal1) TTT GTC GAC TGG TTA GGG CCC TCC ATC. All were cloned in frame into pEYFP-C1 as EcoR1 and Sal1 fragments and confirmed by sequencing. Tagged dynein subunits were described previously [26,43,44]. Cy3-tubulin was prepared as previously described [45].

siRNA depletion

NIH3T3 cells were transfected with siRNA using Lipofectamine RNAiMAX (Invitrogen, Carlsbad, CA) according the manufacturer protocol. The sense sequences for Par3 were: #1 (5′-AGACAGACUGGUAGCAGUATT-3′), #2 (5′-GUGAAAUUGAGGUCACGCCTT-3′) (same sequence as oligonucleotide #4 as perviously described [46]. The sense sequences for LIC1 were: #1 (5′-GUUGAUUAGAGACUUCCAATT-3′), #2 (5′-GUGUGAUGCCAUUAGUGUATT). The sense sequences for LIC2 are: #1 (5′-GCCAGAAGACGCGTATGAATT-3′), #2 (5′-CCAUGACUUUAAUGUAUAATT-3′). SiRNA oligonucleotides were obtained from Sigma or Shanghai GenePharma Co., Ltd (Shanghai, China). Protein levels were analyzed by western blotting using antibodies against Par3, LIC1, LIC2, and mDia1 at 1:1000, GAPDH at 1:2000.

Immunoprecipitation

A 10cm dish of semi-confluent NIH3T3 cells was washed twice in PBS and extracted on ice for 10min in 500 μl of lysis buffer (20 mM Tris at pH 7.4-8.0, 150 mM NaCl, 1% Triton X-100, protease inhibitor cocktail (Sigma) and phosphatase inhibitor cocktail (5 mM β-glycerophosphate, 1 mM sodium orthovanadate, 2.5 mM sodium pyrophosphate)). The lysate was clarified by centrifugation (10min at 13,000g) and immunoprecipitated with 5μg of αDIC mAb 74.1 and protein-G beads (Zymed/Invitrogen) overnight at 4°C. Immunoprecipitated proteins were analyzed by western blotting. For immunoprecipitation of YFP-Par3, COS7 cells were transfected with cDNA for YFP-Par3 using FuGENE^{6} (Roche), and after expression overnight, were extracted as described above and immunoprecipitated using either 5μg rabbit anti-GFP antibody or DIC mAb 74.1 and protein-A beads (Zymed). To detect dynein subunit interactions, YFP-Par3 was co-expressed with tagged dynein subunits in COS7 cells. As

controls, non-immune rabbit or mouse immunoglobulin G were used at the same concentrations as the specific antibodies.

Cell culture, microinjection and immunofluorescence

NIH3T3 cells were cultured in DMEM with 10% calf serum as previously described [47]. For analysis of centrosome orientation, confluent NIH3T3 cells were serum starved for 2 days, wounded, and microinjected as previously described [32]. Purified plasmid DNA was microinjected into nuclei allowed to express for 1-1.5 h as described [2]. Purified αDIC mAb 74.1 (from K. Pfister, University of Virginia) was microinjected into the cytoplasm at 1 mg/ml. Centrosome orientation was induced by adding 10μM LPA to starved cells for 2-2.5h. Cells on coverslips were fixed in -20°C methanol as cribed [2]. Cells were stained with antibodies against tyrosinated tubulin (1:10 of culture supernatant), pericentrin (1:200), Par3 or β-catenin or N-cadherin (all 1:100) for cell outline and DAPI. Secondary antibodies (Cy2, Cy3, Cy5), preabsorbed to minimize species cross-reactivity, were from Jackson ImmunoResearch Laboratories (West Grove, PA).

Analysis of nucleus and centrosome position

Images of cells stained for pericentrin, β-catenin, expression tag (GFP), and MTs were taken on a Nikon Optiphot microscope with a 60X (1.4 NA) Plan Apo objective and a Micromax CCD camera controlled by Metamorph software (Molecular Devices, Phildelphia, PA) as previously described [2]. Centrosome reorientation was determined as previously described [2]. Analysis of nucleus and centrosome positions relative to the cell centroid was adapted from a previous protocol [9,48]. Three independent experiments (≥40 cells) were analyzed for each condition, and error bars in plots are SEM.

Quantification of Par3/MT and Par3/dynein overlap

Serum-starved wound-edge NIH3T3 cells were fixed and stained for Par3, MTs and dynein (αDIC). Images were acquired using a 60x (1.4 NA) Plan Apo objective (Nikon) keeping the exposure constant for each channel and analyzed with MetaMorph. Regions of 100 pixels (6.45μm) diameter (typically 10 regions/cell) were drawn around Par3 positive structures at the cell-cell contacts. Then, images were thresholded on cell-cell contact structures (Par3 and dynein) and MTs. Overlap between Par3 and MT or dynein pixels was then determined using the ‘Measure Colocalization’ function in MetaMorph.

Time-lapse microscopy of MT dynamics

NIH3T3 cells stably expressing EGFP-α-tubulin [9,48] were grown on 35 mm dishes with glass coverslip bottoms. Confluent monolayers were starved for 24 hr in serum-free DMEM. Monolayers were wounded, washed with recording media (Hank’s balanced salt solution (GIBCO) containing essential and nonessential MEM amino acids (GIBCO), 2.5 g/l glucose, 2 mM glutamine, 1 mM sodium pyruvate, and 10 mM HEPES (pH 7.4)) and stimulated with LPA for at least 1h. Cells were imaged on a Nikon TE300 microscope maintained at 36°C using a 100X (1.4 NA) Plan Apo objective (Nikon). Phase-contrast and fluorescence images were collected at 7 sec/frame (200-400 ms/exposure) using a Coolsnap HQ (Roper Scientific) camera controlled by MetaMorph. For experiments with YFP-Par3 expressing cells, cDNAs encoding YFP-Par3 fragments were expressed by microinjection (see above) and then the media was changed to LPA-containing recording media (see above) and Cy3 labeled tubulin (2 mg/ml) was injected into the cytoplasm of expressing cells [45]. Before imaging, 20 mM of Oxyrase (2% vol/vol of the original stock) was added to the media, followed by 3 ml of light mineral oil and incubated for at least 20 min at 37°C to deplete oxygen [45,49].

Analysis of MT dynamics

MT ends were tracked using the 'Track Points' function in MetaMorph. Values logged into Excel and distances were converted from pixels to μm based on the magnification of the 100X objective. A pausing event was assigned for values ≤ +/-0.5μm, a growth event for values > +0.5μm and a shortening event for values < -0.5μm. The percentage of time MTs paused was calculated by dividing the total time of all pausing events by the total observation time. The percentage of pausing lengths longer than 30sec was determined by dividing the total # of pause lengths > 30sec over the total # of pausing periods. MT dynamicity was calculated from the sum of all growth and shortening events per MTs divided by its total observation time. Growth and shortening rates were calculated by dividing the distances for each event by the time interval. Rescue and catastrophe frequencies were obtained by counting the transitions from shortening to growth or pause (rescue) and the transitions from pausing or growth to shortening (catastrophe) and dividing by the total observation time.

Cell migration

NIH3T3 cells cultured in DMEM with 10% serum were transfected with siRNA against GAPDH or Par3 in 35 mm dishes with glass coverslip bottoms using RNAiMAX (Invitrogen). When the monolayers became confluent 2 days later, they were wounded, allowed to recover (~1 hr) and then imaged with a 10× phase objective (Nikon) in bicarbonate-free recording media containing 2% serum on an inverted Nikon TE300 microscope maintained at 36°C equipped with an automated x/y-stage (Prior). At least 10 wounds were monitored for each condition. Phase-contrast images were acquired every 30 min for up to 15 h using the "Multidimensional Acquisition" function of MetaMorph and a Coolsnap HQ camera. Rates of migration were determined by tracing wound edges and determining the average advance of the wound edge. For cells expressing YFP-Par3 fragments, serum-starved wound-edge cells were microinjected with YFP-Par3 205-283 or YPF-Par3-Nt-90 plasmids. After expression (1 hr), cells were stimulated with 2% serum for 12h, then fixed and stained to reveal the expressing cells. Cells that did not maintain contact with the wound edge were scored as having fallen behind the wound edge.

Supplementary Material

Refer to Web version on PubMed Central for supplementary material.

Acknowledgements

We thank V. Rodionov for Cy3-tubulin, R. McKenney for technical assistance with the dynein immunoprecipitation and purified dynein; K. Pfister for the purified αDIC mAb; F. Bartolini and E. Folker for comments on the manuscript; and R.-C. Liu for help on the statistical analysis. This work was supported by NIH grant GM062938 (to G.G.G.), by NIH grant GM47434 (to R.B.V.), by grants from the CIHR, the National Cancer Institute of Canada (to T.P.), and by grants from NSERC (to J.P.F). J.P.F. holds a Tier 2 Canadian Research Chair in Brain Repair.

References

1. Etienne-Manneville S, Hall A. Integrin-mediated activation of Cdc42 controls cell polarity in migrating astrocytes through PKCzeta. Cell 2001;106:489–498. [PubMed: 11525734]
2. Palazzo AF, Joseph HL, Chen YJ, Dujardin DL, Alberts AS, Pfister KK, Vallee RB, Gundersen GG. Cdc42, dynein, and dynactin regulate MTOC reorientation independent of Rho-regulated microtubule stabilization. Curr Biol 2001;11:1536–1541. [PubMed: 11591323]
3. Tsai JW, Bremner KH, Vallee RB. Dual subcellular roles for LIS1 and dynein in radial neuronal migration in live brain tissue. Nat Neurosci 2007;10:970–979. [PubMed: 17618279]
4. Manneville JB, Etienne-Manneville S. Positioning centrosomes and spindle poles: looking at the periphery to find the centre. Biol Cell 2006;98:557–565. [PubMed: 16907664]

5. Li R, Gundersen GG. Beyond polymer polarity: how the cytoskeleton builds a polarized cell. Nature reviews 2008;9:860–873.
6. Bergmann JE, Kupfer A, Singer SJ. Membrane insertion at the leading edge of motile fibroblasts. Proc Natl Acad Sci U S A 1983;80:1367–1371. [PubMed: 6298789]
7. Schmoranzer J, Kreitzer G, Simon SM. Migrating fibroblasts perform polarized, microtubule-dependent exocytosis towards the leading edge. J Cell Sci 2003;116:4513–4519. [PubMed: 14576345]
8. Prigozhina NL, Waterman-Storer CM. Protein kinase D-mediated anterograde membrane trafficking is required for fibroblast motility. Curr Biol 2004;14:88–98. [PubMed: 14738729]
9. Gomes ER, Jani S, Gundersen GG. Nuclear movement regulated by Cdc42, MRCK, myosin, and actin flow establishes MTOC polarization in migrating cells. Cell 2005;121:451–463. [PubMed: 15882626]
10. Dujardin DL, Barnhart LE, Stehman SA, Gomes ER, Gundersen GG, Vallee RB. A role for cytoplasmic dynein and LIS1 in directed cell movement. J Cell Biol 2003;163:1205–1211. [PubMed: 14691133]
11. Burakov A, Nadezhdina E, Slepchenko B, Rodionov V. Centrosome positioning in interphase cells. J. Cell Biol 2003;162:963–969. [PubMed: 12975343]
12. Vallee RB, Stehman SA. How dynein helps the cell find its center: a servomechanical model. Trends Cell Biol 2005;15:288–294. [PubMed: 15953546]
13. Grill SW, Hyman AA. Spindle positioning by cortical pulling forces. Dev Cell 2005;8:461–465. [PubMed: 15809029]
14. Macara IG. Parsing the polarity code. Nature reviews 2004;5:220–231.
15. Etemad-Moghadam B, Guo S, Kemphues KJ. Asymmetrically distributed PAR-3 protein contributes to cell polarity and spindle alignment in early C. elegans embryos. Cell 1995;83:743–752. [PubMed: 8521491]
16. Gonczy P, Pichler S, Kirkham M, Hyman AA. Cytoplasmic Dynein Is Required for Distinct Aspects of MTOC Positioning, Including Centrosome Separation, in the One Cell Stage Caenorhabditis elegans Embryo. The Journal of Cell Biology 1999;147:135–150. [PubMed: 10508861]
17. Grill SW, Gonczy P, Stelzer EH, Hyman AA. Polarity controls forces governing asymmetric spindle positioning in the Caenorhabditis elegans embryo. Nature 2001;409:630–633. [PubMed: 11214323]
18. Labbe JC, Maddox PS, Salmon ED, Goldstein B. PAR Proteins Regulate Microtubule Dynamics at the Cell Cortex in C. elegans. Curr Biol 2003;13:707–714. [PubMed: 12725727]
19. Joberty G, Petersen C, Gao L, Macara IG. The cell-polarity protein Par6 links Par3 and atypical protein kinase C to Cdc42. Nat Cell Biol 2000;2:531–539. [PubMed: 10934474]
20. Lin D, Edwards AS, Fawcett JP, Mbamalu G, Scott JD, Pawson T. A mammalian PAR-3-PAR-6 complex implicated in Cdc42/Rac1 and aPKC signalling and cell polarity. Nat Cell Biol 2000;2:540–547. [PubMed: 10934475]
21. Plant PJ, Fawcett JP, Lin DC, Holdorf AD, Binns K, Kulkarni S, Pawson T. A polarity complex of mPar-6 and atypical PKC binds, phosphorylates and regulates mammalian Lgl. Nat Cell Biol 2003;5:301–308. [PubMed: 12629547]
22. Ligon LA, Karki S, Tokito M, Holzbaur EL. Dynein binds to beta-catenin and may tether microtubules at adherens junctions. Nat Cell Biol 2001;3:913–917. [PubMed: 11584273]
23. Paschal BM, Holzbaur EL, Pfister KK, Clark S, Meyer DI, Vallee RB. Characterization of a 50-kDa polypeptide in cytoplasmic dynein preparations reveals a complex with p150GLUED and a novel actin. J Biol Chem 1993;268:15318–15323. [PubMed: 8325901]
24. Vallee RB, Williams JC, Varma D, Barnhart LE. Dynein: An ancient motor protein involved in multiple modes of transport. J Neurobiol 2004;58:189–200. [PubMed: 14704951]
25. Purohit A, Tynan SH, Vallee R, Doxsey SJ. Direct interaction of pericentrin with cytoplasmic dynein light intermediate chain contributes to mitotic spindle organization. J Cell Biol 1999;147:481–492. [PubMed: 10545494]
26. Tynan SH, Purohit A, Doxsey SJ, Vallee RB. Light intermediate chain 1 defines a functional subfraction of cytoplasmic dynein which binds to pericentrin. J Biol Chem 2000;275:32763–32768. [PubMed: 10893222]

27. Pegtel DM, Ellenbroek SI, Mertens AE, van der Kammen RA, de Rooij J, Collard JG. The Par-Tiam1 complex controls persistent migration by stabilizing microtubule-dependent frontrear polarity. Curr Biol 2007;17:1623–1634. [PubMed: 17825562]
28. Nakayama M, Goto TM, Sugimoto M, Nishimura T, Shinagawa T, Ohno S, Amano M, Kaibuchi K. Rho-kinase phosphorylates PAR-3 and disrupts PAR complex formation. Dev Cell 2008;14:205–215. [PubMed: 18267089]
29. Izumi Y, Hirose T, Tamai Y, Hirai S, Nagashima Y, Fujimoto T, Tabuse Y, Kemphues KJ, Ohno S. An atypical PKC directly associates and colocalizes at the epithelial tight junction with ASIP, a mammalian homologue of Caenorhabditis elegans polarity protein PAR-3. J Cell Biol 1998;143:95–106. [PubMed: 9763423]
30. Waterman-Storer CM, Salmon WC, Salmon ED. Feedback interactions between cell-cell adherens junctions and cytoskeletal dynamics in newt lung epithelial cells. Mol Biol Cell 2000;11:2471–2483. [PubMed: 10888682]
31. Wadsworth P. Regional regulation of microtubule dynamics in polarized, motile cells. Cell Motil Cytoskeleton 1999;42:48–59. [PubMed: 9915584]
32. Cook TA, Nagasaki T, Gundersen GG. Rho guanosine triphosphatase mediates the selective stabilization of microtubules induced by lysophosphatidic acid. J Cell Biol 1998;141:175–185. [PubMed: 9531557]
33. Etienne-Manneville S, Hall A. Cdc42 regulates GSK-3beta and adenomatous polyposis coli to control cell polarity. Nature 2003;421:753–756. [PubMed: 12610628]
34. Heil-Chapdelaine RA, Oberle JR, Cooper JA. The cortical protein Num1p is essential for dynein-dependent interactions of microtubules with the cortex. J Cell Biol 2000;151:1337–1344. [PubMed: 11121446]
35. Ligon LA, Holzbaur EL. Microtubules tethered at epithelial cell junctions by dynein facilitate efficient junction assembly. Traffic (Copenhagen, Denmark) 2007;8:808–819.
36. Harris TJ, Peifer M. The positioning and segregation of apical cues during epithelial polarity establishment in Drosophila. J Cell Biol 2005;170:813–823. [PubMed: 16129788]
37. Tabuse Y, Izumi Y, Piano F, Kemphues KJ, Miwa J, Ohno S. Atypical protein kinase C cooperates with PAR-3 to establish embryonic polarity in Caenorhabditis elegans. Development 1998;125:3607–3614. [PubMed: 9716526]
38. Chen X, Macara IG. Par-3 controls tight junction assembly through the Rac exchange factor Tiam1. Nature Cell Biology 2005;7:262–269.
39. Zhang H, Macara IG. The PAR-6 Polarity Protein Regulates Dendritic Spine Morphogenesis through p190 RhoGAP and the Rho GTPase. Dev Cell 2008;14:216–226. [PubMed: 18267090]
40. Goldstein B, Macara IG. The PAR proteins: fundamental players in animal cell polarization. Dev Cell 2007;13:609–622. [PubMed: 17981131]
41. Drewes G, Ebneth A, Preuss U, Mandelkow EM, Mandelkow E. MARK, a novel family of protein kinases that phosphorylate microtubule-associated proteins and trigger microtubule disruption. Cell 1997;89:297–308. [PubMed: 9108484]
42. Paschal BM, Mikami A, Pfister KK, Vallee RB. Homology of the 74-kD cytoplasmic dynein subunit with a flagellar dynein polypeptide suggests an intracellular targeting function. J Cell Biol 1992;118:1133–1143. [PubMed: 1387402]
43. Tai CY, Dujardin DL, Faulkner NE, Vallee RB. Role of dynein, dynactin, and CLIP-170 interactions in LIS1 kinetochore function. J Cell Biol 2002;156:959–968. [PubMed: 11889140]
44. Tynan SH, Gee MA, Vallee RB. Distinct but overlapping sites within the cytoplasmic dynein heavy chain for dimerization and for intermediate chain and light intermediate chain binding. J Biol Chem 2000;275:32769–32774. [PubMed: 10893223]
45. Semenova I, Rodionov V. Fluorescence microscopy of microtubules in cultured cells. Methods in molecular medicine 2007;137:93–102. [PubMed: 18085223]
46. Nishimura T, Yamaguchi T, Kato K, Yoshizawa M, Nabeshima Y.-i. Ohno S, Hoshino M, Kaibuchi K. PAR-6-PAR-3 mediates Cdc42-induced Rac activation through the Rac GEFs STEF/Tiam1. Nature Cell Biology 2005;7:270–277.
47. Gundersen GG, Kim I, Chapin CJ. Induction of stable microtubules in 3T3 fibroblasts by TGF-beta and serum. J Cell Sci 1994;107:645–659. [PubMed: 8006078]

48. Gomes ER, Gundersen GG. Real time centrosome reorientation during fibroblast migration. Methods in Enzymology 2006;406:579–592. [PubMed: 16472689]

49. Mikhailov AV, Gundersen GG. Centripetal transport of microtubules in motile cells. Cell Motil Cytoskeleton 1995;32:173–186. [PubMed: 8581974]

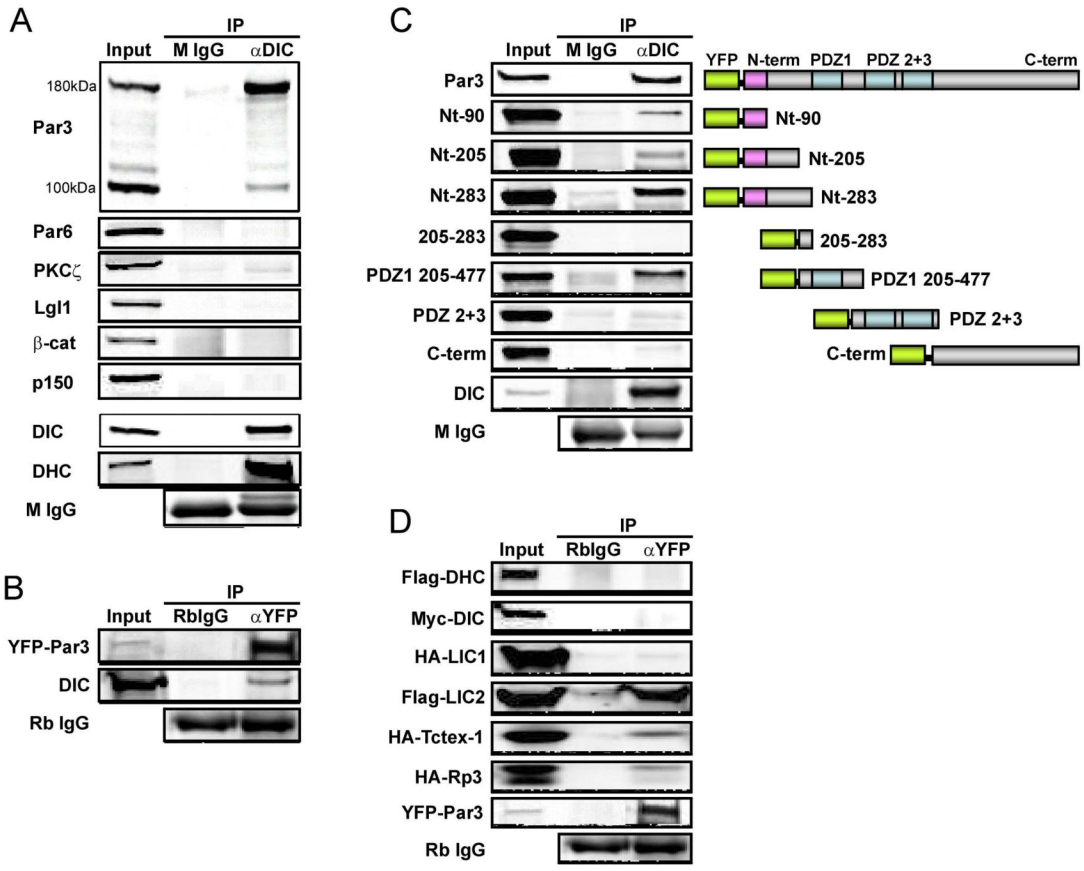

Figure 1. Par3 association with dynein

(A) Dynein immunoprecipitation from lysates of NIH3T3 cells using αDIC or control mouse IgG (MIgG), western blotted for endogenous Par3, Par6, PKCζ, Lgl-1, β-catenin (β-cat) and the p150^{Glued} subunit of dynactin. Immunoprecipitation of dynein was confirmed by western blot for DIC and DHC. Both isoforms of Par3 (180kDa stronger than 100kDa) coimmunoprecipitated with dynein. **(B)** YFP-Par3 immunoprecipitation from lysates of COS-7 cells expressing YFP-Par3 using GFP antibody that recognizes YFP (αYFP) or control rabbit IgG (RbIgG), western blotted for DIC or YFP-Par3. **(C)** Dynein immunoprecipitation from COS-7 cells expressing YFP-Par3 full length (Par3) or fragments as indicated using αDIC or control mouse IgG (MIgG), western blotted for YFP-Par3 and DIC. **(D)** YFP-Par3 immunoprecipitation from COS-7 cells co-expressing YFP-Par3 and Flag-, Myc- or HA-tagged subunits of dynein using GFP antibody (labeled αYFP in figure) or control rabbit IgG (RbIgG). Western blots for dynein subunit tags or YFP-Par3. In A-D, “Input” was 2-4% of total cell lysates.

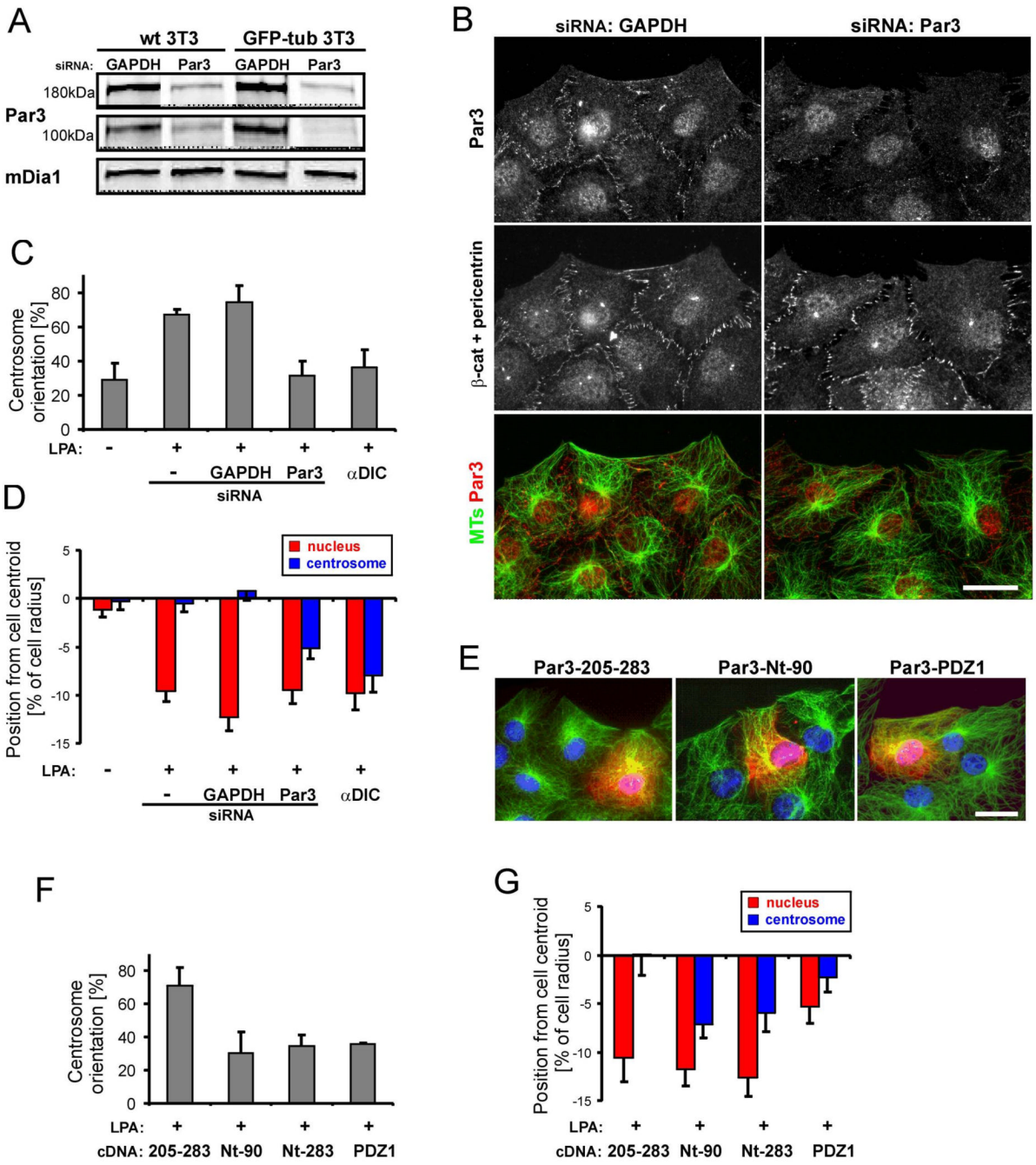

Figure 2. Par3 is necessary for centrosome orientation and centration

(A) Western blots of Par3 and mDia1 (loading control) from NIH3T3 cells (wt and a stable cell line expressing GFP-α-tubulin) treated with siRNAs to Par3 and GAPDH (control). **(B)** Representative images of GAPDH and Par3 siRNA-treated NIH3T3 cells that were wounded, LPA-stimulated and stained for Par3, β-catenin and pericentrin (in one channel), and MTs (shown as an overlay with Par3). Nuclear staining was not reduced by Par3 siRNA suggesting that it is a staining artifact of the commercial antibody. Bar, 20μm. **(C)** Quantification of LPA-stimulated centrosome orientation in GAPDH or Par3 siRNA-treated and αDIC injected cells. Centrosomes were scored as oriented when they were positioned in the triangular sector defined by the nucleus and leading edge [2]. Random centrosome orientation is 33% with these criteria.

(D) Quantification of the position of the nucleus (red) and the centrosome (blue) along the axis of the cell perpendicular to the wound in LPA-stimulated GAPDH and Par3 siRNA-treated cells and αDIC injected cells. The cell center is defined as "0"; (+) values are toward the leading edge and (-) are toward the rear of the cell. Values are plotted as percentage of cell radius to normalize for differences in cell area. **(E)** Representative images of wounded and LPA-stimulated cells expressing a control YFP-Par3 fragment (205-208) and dynein-binding YFP-Par3 fragments (Nt-90, PDZ1). Cells were stained for MTs (green), Par3 tag (red) and DAPI (blue). Bar, 20μm. **(F)** Quantification of LPA-stimulated centrosome orientation in cells expressing Par3 fragments. **(G)** Quantification of the position of the nucleus (red) and the centrosome (blue) as in (D) in LPA-stimulated cells expressing Par3 fragments as indicated. Centrosome orientation data (C,F) and nuclear and centrosome position data (D,G) are based upon at least two separate experiments (N>50 cells for each condition). C,F: error bars = s.d. (N>50 cells for each condition). D,G: error bars = s.e.m.

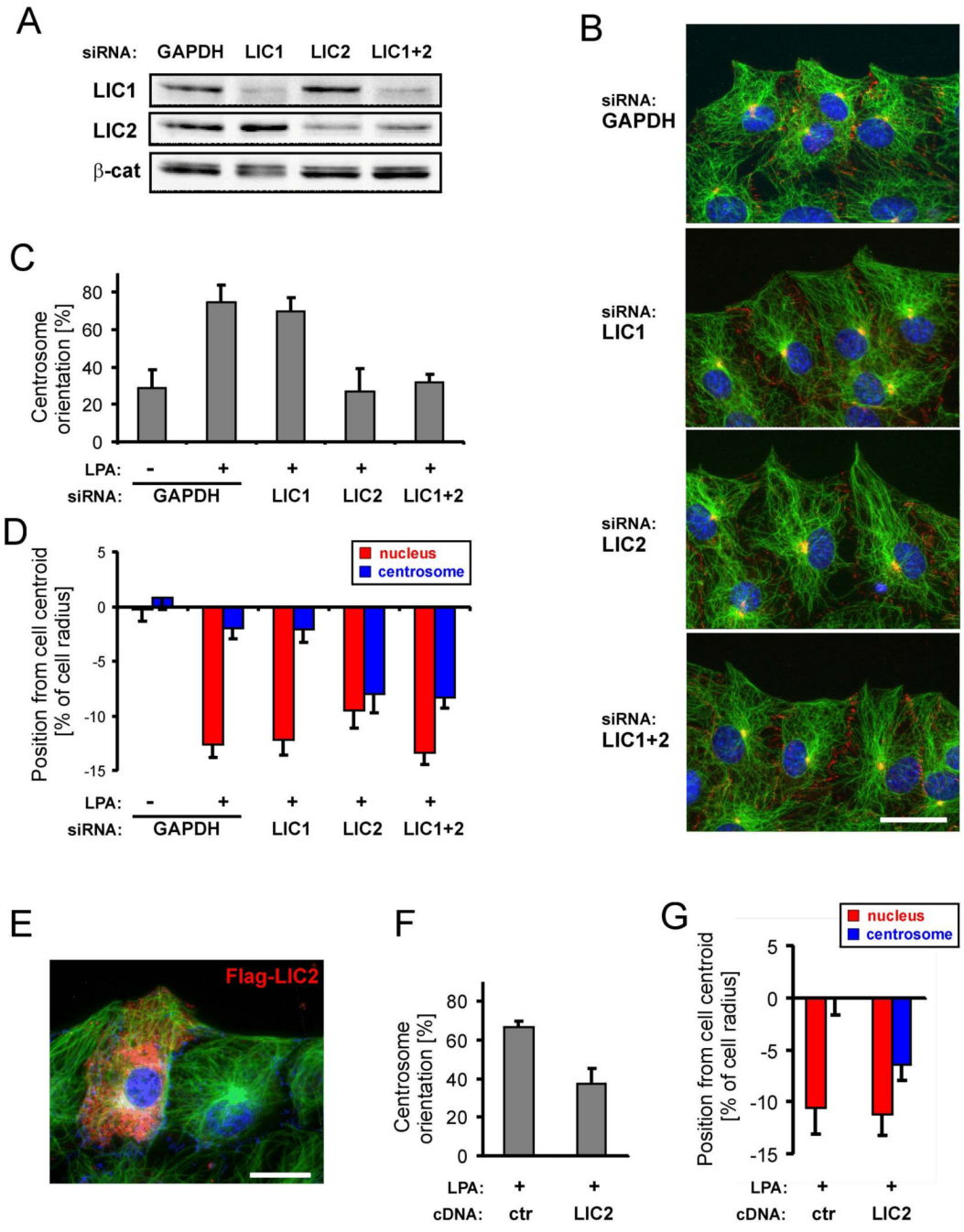

Figure 3. Dynein LIC2 is necessary for centrosome orientation and centration

(A) Western blots of LIC1, LIC2 and β-catenin (100 kDa, loading control) from NIH3T3 cells treated with the indicated siRNAs. See Figure S2 for quantification. **(B)** Representative images of wounded and LPA-stimulated NIH3T3 cells treated with the indicated siRNA. Cells were stained for MTs (green), N-cadherin + pericentrin (red) and DAPI (blue). The centrosome appears as a yellow spot due to overlap of pericentrin and MT staining. Bar, 20μm. **(C)** Quantification of LPA-stimulated centrosome orientation in GAPDH, LIC1 and LIC2 depleted cells. **(D)** Quantification of the position of the nucleus (red) and the centrosome (blue) (as defined in legend of Figure 2D) in LPA-stimulated cells depleted of LIC1, LIC2 or GAPDH (control). . **(E)** Representative image of a wounded and LPA-stimulated NIH3T3 cell

expressing Flag-LIC2. Cells were stained for MTs (green), LIC2 tag (red) and DAPI (blue). Bar, 20μm. **(F)** Quantification of LPA-stimulated centrosome orientation in control GFP (ctr) and Flag-LIC2 expressing NIH3T3 cells. **(G)** Quantification of the position of the nucleus (red) and the centrosome (blue) (as defined in legend of Figure 2D) in LPA-stimulated cells expressing control GFP (ctr) or LIC2 as indicated. Centrosome orientation (C,F) and nuclear/centrosome positioning data (D,G) are based upon at least two separate experiments (N>50 cells for each condition). Error bars = s.e.m.

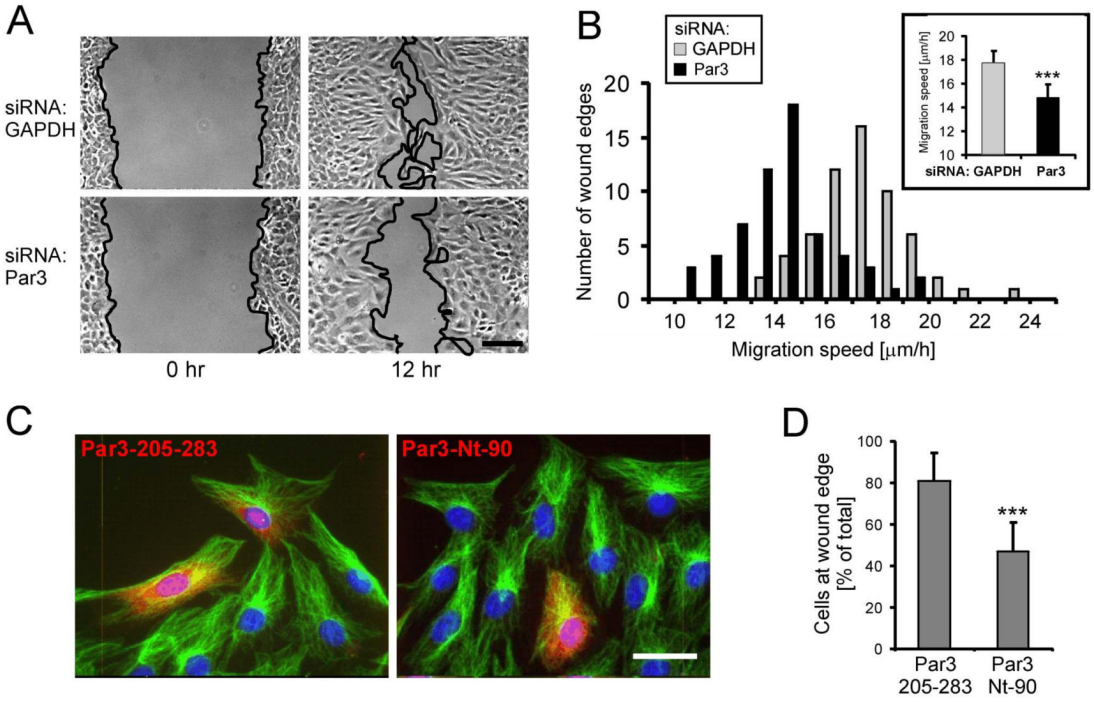

Figure 4. Par3 depletion and dominant negative construct interfere with cell migration

(A) Images from movies of wounded monolayers of NIH3T3 cells that had been treated with siRNA against GAPDH or Par3 and allowed to migrate in the presence of serum. Wound edge is outlined in black. Bar, 100μm. **(B)** Frequency histogram of individual wound edge speeds (binned in 1μm/h intervals) and the average migration speeds (inset histogram) of control GAPDH and Par3 siRNA-treated cells. Data represents 60 wound edges and two independent experiments. Error bars = s.d. Statistical significance was assessed with a two-tailed, unpaired T-test (*** = $p<0.0001$). **(C)** Images of NIH3T3 cells expressing YFP-Par3 205-283 or YFP-Par3 Nt-90 and stimulated to migrate for 15 hr with 2% serum. Cells were stained for GFP (red), MTs (green) and DAPI (blue). Constructs were expressed in wound-edge cells by cDNA microinjection just after wounding. Bar, 20μm. **(D)** Quantification of the wound edge persistence of NIH3T3 cells expressing the indicated Par3 fragments after 15 hr migration in 2% serum. Data are from at least four separate experiments with a total number of injected cells > 50 (error bars = s.d.). Statistical significance was assessed with Chi^2-test (*** = $p<0.0001$).

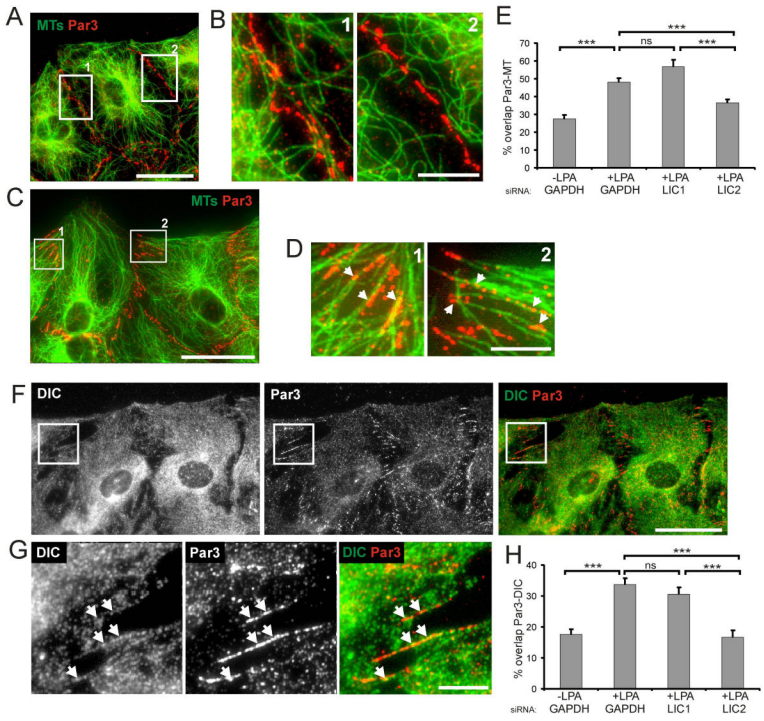

Figure 5. Par3 localizes to cell-cell contacts of wound-edge NIH3T3 cells where it overlaps with MT ends and dynein

(A) Untreated and **(C)** LPA-stimulated woundedge NIH3T3 cells stained for MTs (green) and endogenous Par3 (red). Bar, 20μm. **(B,D)** High magnification of boxed regions labeled "1" and "2" in A and C. Bar, 5 μm. Arrows indicate puncta of Par3 that colocalize with MT ends. **(E)** Quantification of Par3 overlap with MTs at cell-cell contacts in cells treated with the indicated siRNAs and stimulated with LPA. **(F,G)** Wounded and LPA-stimulated NIH3T3 cells stained for DIC and Par3. **(F)** Low magnification view showing punctate DIC distribution throughout the cytosol with accumulations in the perinuclear area and the leading edge. Bar, 20μm. **(G)** Higher magnification of boxed region in F. Arrows indicate overlapping puncta of DIC and Par3. Bar, 5μm. **(H)** Quantification of Par3 overlap with DIC at cell-cell contacts in cells treated with the indicated siRNAs and stimulated with LPA. Data (E,H) are from two independent experiments in which more than 100 regions from 10-15 images were analyzed. Error bars = s.e.m. Statistical significance was assessed with a two-tailed, unpaired T-test (*** = $p<0.0001$; ns =not significant).

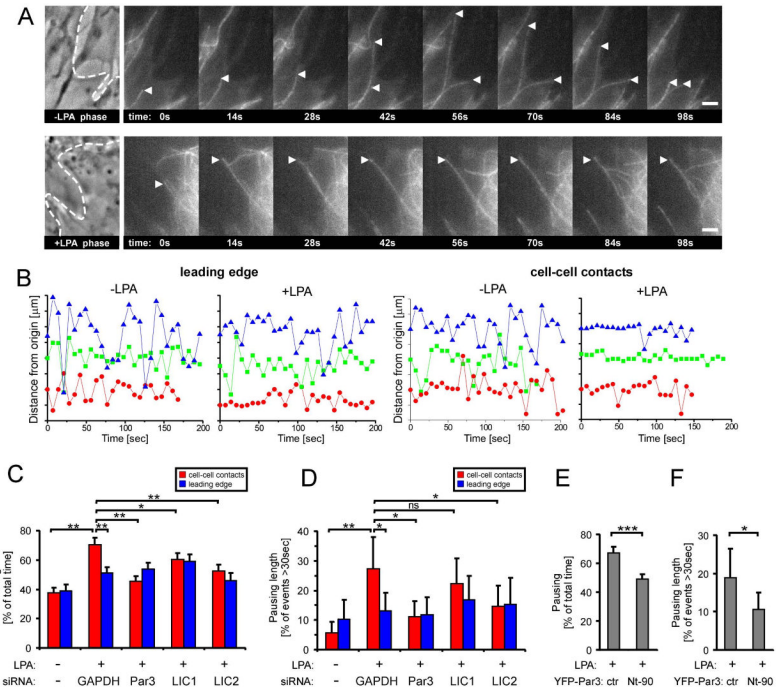

Figure 6. LPA stimulates Par3 and LIC2 dependent pausing of MTs at the cell-cell contacts

(A) Frames from movies of GFP-α-tubulin expressing NIH3T3 cells showing examples of MT dynamics at regions of cell-cell contact before (-LPA) and after stimulation with LPA (+LPA). The first panel shows a phase image from the beginning of the movie (dashed line denotes cell-cell contact). Arrowheads indicate MTs that exhibit dynamic instability in unstimulated cells (-LPA) and a MT that pauses for 84 sec (frames 14-98s) in an LPA-stimulated cell (+LPA). Bars, 2µm. **(B)** Life history plots (distance vs. time) for 3 MT ends at the leading edge and cell-cell contacts of GFP-α-tubulin expressing NIH3T3 cells before (-LPA) and after stimulation with LPA (+LPA). **(C)** Quantification of time MTs spent pausing and **(D)** MTs that exhibited long pause intervals (>30 sec) at cell-cell contacts and the leading edge from GFP-α-tubulin expressing NIH3T3 cells treated as indicated. Data for each condition are pooled from 4-8 different cells (2-3 independent experiments) and 25-47 MTs. **(E)** Quantification of time MTs spent pausing and **(F)** MTs that exhibited long pause intervals (>30 sec) at cell-cell contacts of Cy3-tubulin injected cells expressing YFP-Par3 205-283 (ctr) and Nt-90 fragments. Data for each condition are from 6-10 different cells (2 independent experiments) and 23-46 total MTs. In C-F, error bars are the 95% confidence intervals. Statistical significance was assessed with Fisher exact test (* = $p<0.05$, ** = $p<0.001$, ***=$p<0.0001$, “ns” is not significant).